Field-induced dynamics and structures in a cholesteric-blue-phase cell

Jun-ichi Fukuda (福田順一)[1,2,3,*] and Slobodan Žumer[2,3,4]

[1]*Nanosystem Research Institute, National Institute of Advanced Industrial Science and Technology (AIST), 1-1-1 Umezono, Tsukuba 305-8568, Japan*

[2]*Department of Physics, University of Ljubljana, Jadranska 19, 1000 Ljubljana, Slovenia*

[3]*Center of Excellence NAMASTE, Jamova 39, 1000 Ljubljana, Slovenia*

[4]*Jožef Stefan Institute, Jamova 39, 1000 Ljubljana, Slovenia*

(Received 26 February 2013; published 22 April 2013)

We investigate numerically the relaxational dynamics of the orientational order of a cholesteric blue phase (BP) in a planar cell enforcing normal alignment in response to the application and cessation of an external electric field. We focus on the cases where blue phase I (BP I) is stable in the bulk. We show how the reorganization processes of the network of disclinations depend on the field strength and the history of the application of the field. We also demonstrate that the relaxation processes following the cessation of the field are particularly complex and depend sensitively on the profile of the orientational order before the cessation of the field.

DOI: 10.1103/PhysRevE.87.042506 PACS number(s): 61.30.Dk, 61.30.Jf, 61.30.Mp, 61.72.Lk

I. INTRODUCTION

Cholesteric blue phases [1,2] are exotic three-dimensional ordered structures formed by highly chiral liquid crystals. Cholesteric blue phases are optically isotropic; they do not show birefringence. Nevertheless, they show Bragg reflections, which suggests a periodic structure. These specific optical properties attracted academic interest in the 1980s and 1990s, and thus extensive studies were carried out to elucidate the structural properties of cholesteric blue phases. Two of the three bulk blue phases identified so far possess cubic symmetry; the symmetry of blue phase I (BP I) is $O_8(I4_132)$, and that of blue phase II (BP II) is $O_2(P4_232)$ (the structure of blue phase III (BP III) is still under debate, although an amorphous structure is likely [3]). It was demonstrated that BP I and BP II are made up of an intricate network of topological line defects, or disclination lines of winding number $-1/2$, and the so-called double-twist cylinders, in which the nematic director $\boldsymbol{n}$ adopts twist distortions along all the directions normal to the cylinder axis. Cholesteric blue phases have thus drawn attention as an intriguing example of frustration-induced structures; double-twist ordering can be shown to be unable to fill the whole space without introducing singularities [1].

In conventional liquid crystal materials exhibiting cholesteric blue phases, the temperature range of their thermodynamic stability is limited to a few Kelvin, which hindered their use in practical applications. However, Kikuchi and coworkers demonstrated that the introduction of a polymer network by photopolymerization drastically stabilizes cholesteric blue phases and that their stability range can be larger than 60 K [4]. Subsequently, several liquid crystal molecules were shown to exhibit blue phases over a wide temperature range [5,6]. These findings motivated a number of studies aimed at the practical applications of cholesteric blue phases, including lasers [7,8] and fast-switching displays [9–11].

Most of the applications make use of a structural change of cholesteric blue phases under an electric field. Electric-field-induced birefringence, or the optical Kerr effect, is utilized in displays for the switching between off and on states [11,12]. Therefore, understanding how cholesteric blue phases respond to an electric field is an important issue in practical applications as well as in academic research. Field-induced switching between various stable and metastable states of thin layers of a simple cholesteric is well known and has led to numerous applications [13]. Around two decades ago, electrostrictions (variation of the lattice constants due to an applied field) and change in the symmetry of cholesteric blue phases under an electric field were extensively investigated [14]. More recently, simulations studies were devoted to the understanding of the properties of cholesteric blue phases [3,15,16]. Some studies successfully reproduced the experimentally observed electrostrictions and gave more insight into the deformation and reorganization of disclination lines in response to an electric field [17–19]. However, most of the previous numerical studies concerned bulk properties and only very few studies [20,21] addressed the effect of an electric field on cholesteric blue phases in planar cells. In our previous studies, we showed that strong spatial confinement drastically influences the orientational ordering of cholesteric blue phases, yielding various exotic defect structures [22–25]. We also clarified the effect of strong surface anchoring by demonstrating a discretized ordering (that is, the number of double-twist cylinders per thickness must be an integer) which leads to an oscillatory structural force between parallel surfaces of the cell [26]. Therefore we believe that there still remains much to be investigated on how cholesteric blue phases in a cell, not in the bulk, behave in response to an electric field.

In this paper, we carry out simulation studies on the behavior of cholesteric blue phases in a planar cell when an electric field is applied between confining plates. Our simulations are based on the Landau–de Gennes continuum theory which describes the orientational order of a liquid crystal using a second-rank tensor. We are interested in a case where BP I is stable in the bulk and the cell surfaces impose strong (but not perfect) homeotropic anchoring. The cell is thick enough to accommodate a disclination network resembling that of bulk BP I. In our previous paper [21], we presented some preliminary results and here we consider in more detail the effect of the variation of the field strength

*fukuda.jun-ichi@aist.go.jp

and the history of the application of the electric field; we also investigate how the cell relaxes when the electric field is switched off.

II. MODEL

As noted in the Introduction, in our numerical calculations the orientational order is described by a symmetric and traceless second-rank tensor $Q_{\alpha\beta}$. We consider a parallel cell whose confining surfaces are parallel to the xy plane, and located at $z=0$ and $z=d$. The total free energy of our cholesteric blue phase cell as a functional of $Q_{\alpha\beta}$ is formally written as $F=\int dx\,dy\,[\int_0^d dz\{f_{\rm local}(Q_{\alpha\beta})+f_{\rm grad}(Q_{\alpha\beta},\nabla)+f_E(Q_{\alpha\beta},\phi)\}+f_{s0}(Q_{\alpha\beta})+f_{sd}(Q_{\alpha\beta})]$. Here and in the following we adopt the forms of the free energy densities given in Ref. [1], and the local energy density given by a Landau expansion up to fourth order,

$$f_{\rm local}(Q_{\alpha\beta})=c\,{\rm Tr}\mathbf{Q}^2-\sqrt{6}b\,{\rm Tr}\mathbf{Q}^3+a({\rm Tr}\mathbf{Q}^2)^2 \tag{1}$$

takes care of the phase transition due to temperature change, and Tr denotes the trace of a tensor. The parameters $a(>0)$, b, and c depend on the material and the temperature, and in the usual Landau theory, only c is assumed to be temperature dependent (the temperature dependence of a and b does not play an important role and is neglected). The free energy density due to the inhomogeneity of the orientational order, or nonzero $\nabla Q_{\alpha\beta}$, is characterized by two elastic constants and a chiral term

$$\begin{aligned}f_{\rm grad}(Q_{\alpha\beta},\nabla)=&\tfrac{1}{4}K_1[(\nabla\times\mathbf{Q})_{\alpha\beta}+2q_0Q_{\alpha\beta}]^2\\&+\tfrac{1}{4}K_0[(\nabla\cdot\mathbf{Q})_\alpha]^2.\end{aligned} \tag{2}$$

Here using two elastic constants, K_0 and K_1 allows the separate treatment of twist deformation, and $2\pi/|q_0|$ is the pitch characterizing the spontaneous cholesteric twisting. The contribution of the electric field $E=-\nabla\phi$ is given by

$$f_E(Q_{\alpha\beta},\phi)=-\tfrac{1}{2}\epsilon_{\alpha\beta}\nabla_\alpha\phi\nabla_\beta\phi=-\tfrac{1}{2}\epsilon_{\alpha\beta}E_\alpha E_\beta, \tag{3}$$

where ϕ is the electrostatic potential and $\epsilon_{\alpha\beta}$ is the dielectric tensor that depends on $Q_{\alpha\beta}$ (see below). We denote the contribution from the surface anchoring at $z=0$ and d by f_{s0} and f_{sd}, respectively. Their explicit form is

$$f_{s0,d}(Q_{\alpha\beta})=\tfrac{1}{2}W{\rm Tr}(Q-Q_s)^2, \tag{4}$$

where W characterizes the anchoring strength, and $Q_{s\alpha\beta}=Q_0[\nu_\alpha\nu_\beta-(1/3)\delta_{\alpha\beta}]$ defines the order parameter preferred by the surface. In the present study, we consider the case of normal anchoring, and the unit vector ν is taken along the surface normal (or the z direction).

Now we rescale the length so that it is measured in units of $(2q_0)^{-1}$ and then the rescaled cholesteric pitch is 4π. We further introduce the rescaled order parameter $\chi_{\alpha\beta}\equiv(a/b)Q_{\alpha\beta}$, and the free energy densities $\varphi_{{\rm local,grad},E}\equiv(a^3/b^4)f_{{\rm local,grad},E}$ and $\varphi_s\equiv(2q_0)(a^3/b^4)f_s$. The rescaled total free energy is given by $\mathcal{F}\equiv(2q_0)^3(b^4/a^3)F_{\rm tot}=\int d\bar{x}d\bar{y}[\int_0^{\bar{d}}(\varphi_{\rm local}+\varphi_{\rm grad}+\varphi_E)+\varphi_{s0}+\varphi_{sd}]$ with

$$\varphi_{\rm local}(\chi_{\alpha\beta})=\tau\,{\rm Tr}\chi^2-\sqrt{6}\,{\rm Tr}\chi^3+({\rm Tr}\chi^2)^2, \tag{5}$$

$$\varphi_{\rm grad}(\chi_{\alpha\beta},\overline{\nabla})=\kappa^2\{[(\overline{\nabla}\times\chi)_{\alpha\beta}+\chi_{\alpha\beta}]^2+\eta[(\overline{\nabla}\cdot\chi)_\alpha]^2\}, \tag{6}$$

$$\varphi_s=\tfrac{1}{2}w{\rm Tr}(\chi-\chi_s)^2. \tag{7}$$

Here $\bar{x}\equiv(2q_0)x$ and so on are rescaled lengths, $\overline{\nabla}=(2q_0)^{-1}\nabla$, and τ, κ, w are the rescaled temperature, the strength of chirality, and the rescaled anchoring strength, respectively. η represents the inherent anisotropy of liquid crystal elasticity, though we simply set η to 1, which corresponds to the so-called one-constant approximation. The rescaling employed here is the same as that in Wright and Mermin [1] and our previous study [22–25], and see the Appendix for more details of the rescaling.

Following the spirit of de Gennes [27], we assume the linear dependence of the dielectric tensor $\epsilon_{\alpha\beta}$ on $\chi_{\alpha\beta}$ so that the rescaled electrostatic energy density reads

$$\varphi_E=-\tfrac{1}{2}(\epsilon_{\rm iso}\delta_{\alpha\beta}+\epsilon_a\chi_{\alpha\beta})\overline{E}_\alpha\overline{E}_\beta, \tag{8}$$

where $\overline{E}=-\overline{\nabla\phi}$ is the rescaled electric field with $\overline{\phi}$ being the rescaled potential, and ϵ_a is the dielectric anisotropy. When $\epsilon_a>0$ (<0) the liquid crystals tend to align parallel (perpendicular) to the electric field, and here only the cases of positive ϵ_a are considered. How to rescale ϕ and E is given in the Appendix.

We assume that simple relaxational dynamics is given by the following equation for $\chi_{\alpha\beta}$:

$$\tau_\chi\frac{\partial}{\partial t}\chi_{\alpha\beta}=-\left(\frac{\delta\mathcal{F}}{\delta\chi_{\alpha\beta}}+\lambda\delta_{\alpha\beta}\right). \tag{9}$$

Here τ_χ, estimated to be $\simeq 1\,\mu$s [18], is the characteristic time of the rotational relaxation of $\chi_{\alpha\beta}$ that is proportional to the rotational viscosity. The second term ensures the tracelessness of χ and λ is the Lagrange multiplier. We employ an explicit Euler scheme [28] in the integration of Eq. (9). To reduce the numerical cost, a hydrodynamic flow is not taken into account, though it could affect the kinetic pathway of relaxation (in previous similar studies [20] no significant qualitative changes in the dynamics of cholesteric blue phases have been reported).

The electrostatic potential $\overline{\phi}$ obeys the Maxwell equation, which reads

$$\frac{\delta\mathcal{F}}{\delta\overline{\phi}}=\overline{\nabla}_\alpha[(\epsilon_{\rm iso}\delta_{\alpha\beta}+\epsilon_a\chi_{\alpha\beta})\overline{\nabla}_\beta\overline{\phi}]=0. \tag{10}$$

We consider the case in which the confining surfaces are covered with electrodes imposing fixed $\overline{\phi}$, and therefore we solve Eq. (10) under the boundary conditions $\overline{\phi}=0$ at $\bar{z}=0$ and $\overline{\phi}=\overline{\phi}_0$ at $\bar{z}=\bar{d}$. As we show in the Appendix, the relation between the (unrescaled) average field E in V/μm and $\overline{\phi}_0$ becomes

$$\overline{\phi}_0/\bar{d}=2.7\times10^{-2}E. \tag{11}$$

In Sec. III we present our results with the variation of E. We employ a multigrid method [28,29] for efficiently solving Eq. (10). We set $\epsilon_{\rm iso}=10$ and $\epsilon_a=\pm10$ (see the Appendix for the reason of this choice).

In the present study, we choose $\tau = -1$, $\kappa = 0.7$, and $w = 2.5$, which corresponds to setting $2\pi/q_0 \simeq 161$ nm (cholesteric pitch) and $W = 1 \times 10^{-3}$ Jm^{-3} (anchoring strength), though the relation between rescaled and dimensional parameters sensitively depends on the material parameters chosen. See the Appendix for the rescaling. The anchoring strength is large but experimentally achievable. In our previous study [18], we confirmed that, with this choice, BP I is the most stable when confining surfaces are absent. The lattice constant of bulk BP I is 12.60 in the rescaled unit, almost equal to the natural cholesteric pitch (4π). We choose $\chi_0 = 1.44$ so that χ_s minimizes $\varphi_{\rm local}$.

As the initial condition, we employ the profile of a chiral liquid crystal in a parallel cell of thickness $\overline{d} = 33$ ($\simeq$420 nm in real units and approximately 2.6 times the unit cell dimension of BP I) that was obtained in our previous study [26] using the same parameters τ, κ, η, and w. The structure of the disclination lines in the middle of the system closely resembles that of bulk BP I, and the [001] direction is parallel to the surface normal. One can regard this disclination line network as that of 2 BP I unit cells in the z direction. Our previous calculation was performed on a $32 \times 32 \times (64 + 1)$ lattice with periodic boundary conditions along the x and y directions. To reduce possible finite size effects, the present calculations are carried out on a $256 \times 256 \times (64 + 1)$ lattice with the initial condition being a 8×8 repetition of the profile obtained in our previous calculation. In contrast to our previous studies [18] dealing with a single unit cell of cholesteric blue phases or associated defect structures, here we do not change the grid spacings of the numerical system to find a state that minimizes the total free energy. This is because it is practically impossible to find the optimum grid spacings in some cases, in particular, when the liquid crystal is uniformly aligned along a strong field, or it exhibits entangled disclination lines as we will discuss below. We also incorporate small randomness in the initial condition by adding a random number distributed uniformly in the range $[-0.05, 0.05]$ to each component of $\chi_{\alpha\beta}$ at each lattice point and making $\chi_{\alpha\beta}$ at each lattice point traceless. Without this randomness, we would be simulating 8×8 simulations of the same system connected by periodic boundary conditions. As we will see below, small randomness remaining in the course of relaxation plays an important role in the nucleation of defects after a strong field aligning the liquid crystal is switched off. No thermal fluctuations are included in the dynamics.

III. RESULTS AND DISCUSSION

In our numerical calculations we are interested in the cases where an applied electric field induces a recognizable change in the profile of disclinations. In the following, we present results for $E = 10$, 15, and 20 V/μm.

To discuss the dynamical behavior of the system quantitatively, we introduce $\overline{\chi}_{zz} = \int d\overline{\boldsymbol{r}}\, \chi_{zz} / \int d\overline{\boldsymbol{r}}$, as a simple measure of anisotropy. We also calculate the rescaled total energy per unit area $\mathcal{F}/\overline{A} = \overline{A}^{-1} \int d\bar{x} d\bar{y} [\int_0^{\bar{d}} (\varphi_{\rm local} + \varphi_{\rm grad} + \varphi_E) + \varphi_{s0} + \varphi_{sd}]$, with $\overline{A}$ being the rescaled area of one of the confining surfaces, and each contribution from the local, gradient, electrostatic, and anchoring energies defined by $\mathcal{F}_{\rm local}/\overline{A} = \overline{A}^{-1} \int d\bar{x} d\bar{y} \int_0^{\bar{d}} \varphi_{\rm local}$, $\mathcal{F}_{\rm grad}/\overline{A} = \overline{A}^{-1} \int d\bar{x} d\bar{y} \int_0^{\bar{d}} \varphi_{\rm grad}$, $\mathcal{F}_E/\overline{A} = \overline{A}^{-1} \int d\bar{x} d\bar{y} \int_0^{\bar{d}} \varphi_E$, and $\mathcal{F}_s/\overline{A} = \overline{A}^{-1} \int d\bar{x} d\bar{y} [\varphi_{s0} + \varphi_{sd}]$, respectively.

A. Dynamics after the field is switched on

In Figs. 1(a) to 1(c), we show how the disclination network evolves when an electric field $E = 10$ V/μm is applied. Here and in the following we draw isosurfaces of $\mathrm{Tr}\chi^2 = 0.8$ and identify disclinations with weaker orientational order as regions with smaller $\mathrm{Tr}\chi^2$. The disclination network shrinks along the direction of the cell surface normal, or the field direction, though its topology remains unchanged. In Figs. 1(d) and 1(e), we also show the orientation profile at $t/\tau_\chi = 0$ and 396 at a plane perpendicular to the confining surfaces and parallel to the plane of the page. Here and in the following similar figures, we illustrate the direction of an eigenvector of $\chi_{\alpha\beta}$ with the largest eigenvalue. One can identify double-twist cylinders with their axis being normal to the plane of the page, together with surface disclinations that are allowed because the surface anchoring is not perfect but finite. The alignment of the liquid crystal along the electric field is more enhanced near the confining surfaces. It is interesting to note that previous experimental [14] and numerical [17,18] studies concerning the electrostriction of blue phases demonstrate that bulk BP I is compressed along the field direction when the field is applied along the [001] direction, and $\epsilon_a > 0$. Our present result, the compression of the disclination network along the field direction, is consistent with that of bulk electrostriction. Our previous result [18] indicates that the compression of bulk BP I along the field direction with $E = 10$ V/μm is approximately 7.6% (see Fig. 2(a) of Ref. [18], where $\tilde{\epsilon} \simeq 0.2$ corresponds to $E = 10$ V/μm). The compression of the disclination network in Fig. 1, though it is not easy to quantify, looks much larger than 7.6% [30]. The enhanced alignment of the liquid crystal near confining surfaces along the field is expected to give an additional contribution to the compression of the disclination network. We present in Fig. 1(f) the isosurfaces of $\overline{\phi}$. The isosurfaces are almost flat, indicating almost a uniform electric field, though a closer inspection reveals that they deviate very slightly from flat planes.

When a stronger field is applied, the topology of disclination lines can no longer remain intact, and a significant change is observed, as shown in Figs. 2(a) to 2(e) for $E = 15$ V/μm. The complex reorganization of disclination lines is clearly visible, and disclination lines are no longer straight but undulating and confined in a thinner region around the midplane of the cell. The orientation profile when the system is sufficiently relaxed is given in Fig. 2(f). In contrast to the previous case of $E = 10$ V/μm [Fig. 1(e)], the electric field is strong enough to eliminate double-twist cylinders. In particular, near the confining surfaces, the orientation profile is almost that of a cholesteric phase of a single twist with its pitch axis being parallel to the confining surfaces and to the plane of the page. A perfect single twist does not allow disclination lines inside, and therefore the disclination lines are localized around the midplane. The structure observed here might be a metastable state because a cholesteric-like single-twist order without

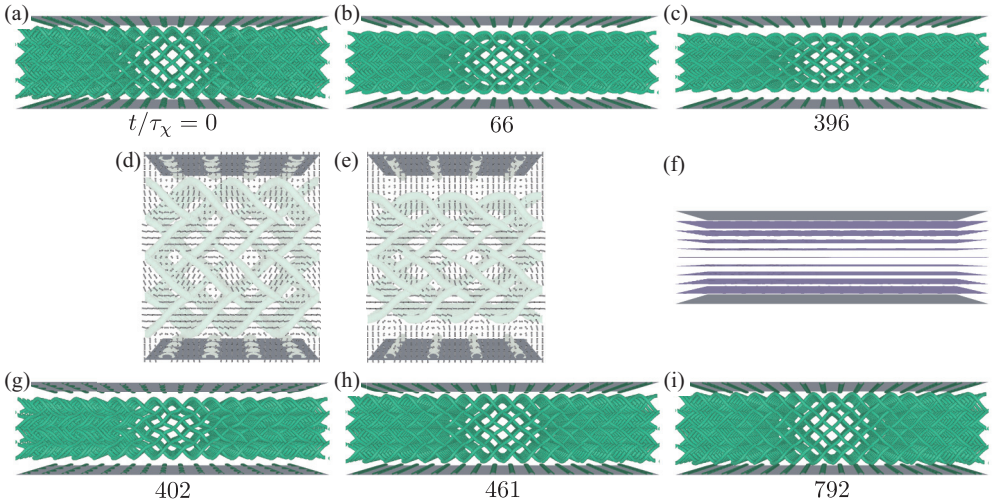

FIG. 1. (Color online) (a–c) Time evolution of disclination lines when $E = 10$ V/μm is applied at $t/\tau_\chi = 0$. (d,e) Orientation profiles at $t/\tau_\chi =$ (d) 0 and (e) 396. For visibility, only a part of the system is shown, and disclination lines are drawn translucently. (f) Isosurfaces of $\overline{\phi} = m\overline{\phi}_0/10$ with $m = 1,2,\ldots,9$ at $t/\tau_\chi = 396$. (g–i) Time evolution of disclination lines after the field is switched off at $t/\tau_\chi = 396$. Here and in Figs. 2 and 3, numbers indicate t/τ_χ after the field is switched on.

disclination is likely to be more energetically favorable. However, the transition to a cholesteric phase is not observed in our calculation. We also note that the applied field is not strong enough to unwind the single-twist helical order of the liquid crystal. All the structures mentioned above (the initial structure [Fig. 1(a)], those sufficiently after the field is switched on [Figs. 1(c) and 2(e)], and those sufficiently after the field is switched off [Figs. 1(i) and 2(i)]) have $p2$ symmetry in two dimensions along the xy plane. (Note the absence of mirror symmetry because of the chirality. The absence of three-, four-, and six-fold symmetry is also obvious from the presence of surface defects.)

An even stronger field eventually removes the disclination lines and the system ends up with a uniform alignment along the field direction without any disclinations, as shown in Figs. 3(a) to 3(f) for $E = 20$ V/μm. The process of the annihilation of disclinations in response to the applied field involves deformation [Fig. 3(b)] and the merging [Fig. 3(c)] of disclination lines and is again quite complex.

In Fig. 4, we plot the time evolution of $\overline{\chi}_{zz}$. Though a bulk BP before the application of the electric field would yield $\overline{\chi}_{zz} = 0$ because of the cubic symmetry, in our cell $\overline{\chi}_{zz}$ before the application of the electric field is $0.082 \neq 0$ because confining surfaces breaks the cubic symmetry of a bulk BP [22]. One can clearly see that $\overline{\chi}_{zz}$ grows more rapidly when the field is stronger. A closer inspection reveals the time evolution of $\overline{\chi}_{zz}$ for $E = 15$ V/μm is not smooth; kinks in the graph signify the change in the topology of the disclination network.

In Fig. 5 we show the time evolution of $\mathcal{F}$'s for different field strengths. In all cases, the abrupt drop of $\mathcal{F}$'s (in particular $\mathcal{F}_{\rm grad}$) just after the application of the electric field at $t/\tau_\chi = 0$ is attributed to the higher free energy of the initial condition and its immediate relaxation because of the introduction of

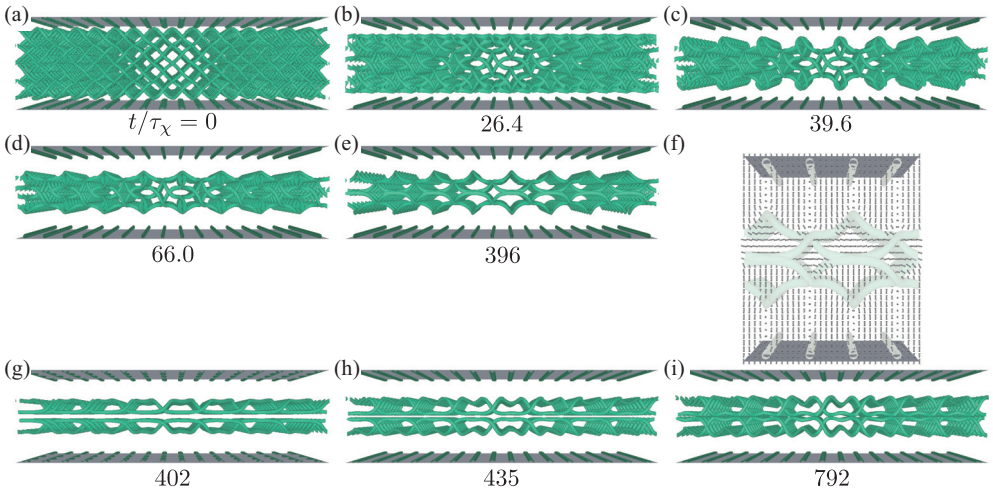

FIG. 2. (Color online) (a–e) Time evolution of disclination lines when $E = 15$ V/μm is applied at $t/\tau_\chi = 0$. (f) Orientation profiles at $t/\tau_\chi = 396$. (g–i) Time evolution of disclination lines after the field is switched off at $t/\tau_\chi = 396$.

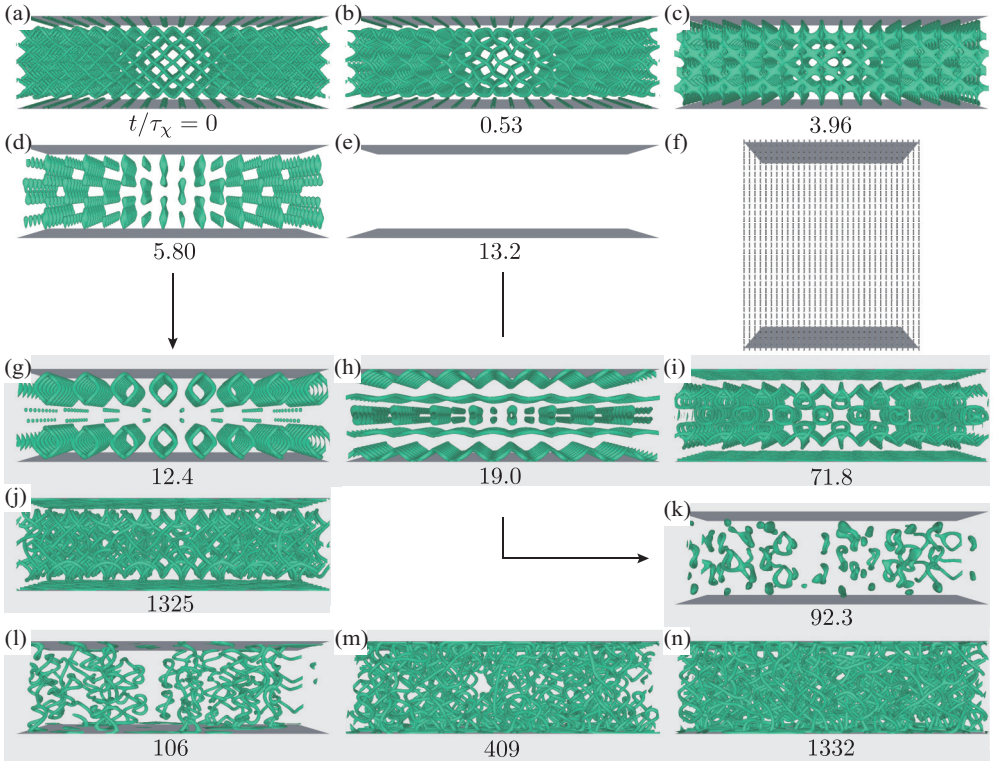

FIG. 3. (Color online) (a–e) Time evolution of disclination lines when $E = 20$ V/μm is applied at $t/\tau_\chi = 0$, 0.53, 3.96, 5.80, and 13.2. (f) Orientation profiles at $t/\tau_\chi = 13.2$. (g–j) Time evolution of disclination lines after the field is switched off at $t/\tau_\chi = 5.80$. (k–n) Time evolution of disclination lines after the field is switched off at $t/\tau_\chi = 13.2$.

randomness as mentioned at the end of Sec. II. It can be seen that the variation of $\mathcal{F}_{\text{total}}$ is dominated by that of $\mathcal{F}_{\text{grad}}$ and $\mathcal{F}_E$ (note the scale of vertical axes). In the case of $E = 10$ V/μm [Fig. 5(a)], the variation of $\mathcal{F}_{\text{local}}$ is almost invisible except at the beginning, while in the cases of stronger field [Figs. 5(b) and 5(c)], the notable change of $\mathcal{F}_{\text{local}}$ can be found, which reflects the disappearance of the disclination lines shown in Figs. 2 and 3. The reorganization of disclination networks marks a small kink in the time evolution of $\mathcal{F}_{\text{grad}}$ as in that of

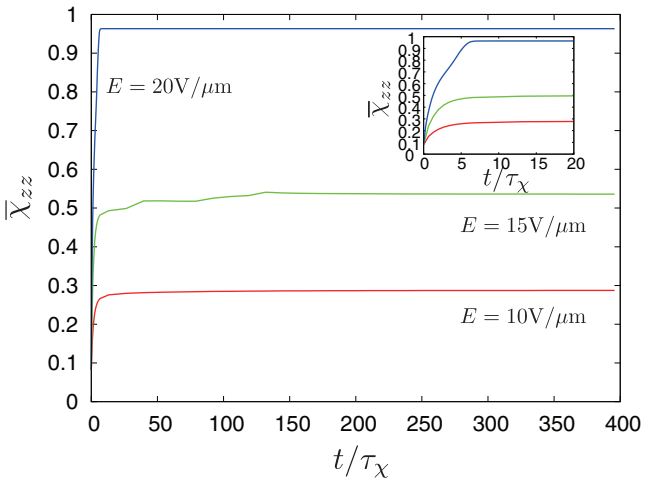

FIG. 4. (Color online) Time evolution of $\overline{\chi}_{zz}$ for $E = 10$, 15, and 20 V/μm from bottom to top. Inset shows the initial stage from $t/\tau_\chi = 0$ to 20.

$\overline{\chi}_{zz}$. We also note that the value of $\mathcal{F}_s$ after sufficient relaxation is smaller for larger E. This is because the normal alignment of the liquid crystal by the electric field is favorable to the surfaces imposing normal anchoring. For $E = 20$ V/μm, $\mathcal{F}_s$ becomes almost zero because of the disappearance of surface disclinations (Fig. 3).

B. Dynamics after the field is switched off

It is also interesting how the liquid crystals behave when an electric field is switched off. In Figs. 1(g) to 1(i), we show the relaxation of the system when the field $E = 10$ V/μm is switched off from the state presented in Fig. 1(c). As expected, the compressed disclination network expands and its final profile is the same as the initial profile before the application of the field.

On the other hand, in the case of $E = 15$ V/μm, the disclination profile sufficiently relaxed after the field is switched off is no longer the initial one, but slight dilations of the disclination network around the midplane are observed as shown in Figs. 2(g) to 2(i). In additional calculations not shown here, we find that when the same field $E = 15$ V/μm is applied to the profile of Fig. 2(i), the liquid crystal recovers the profile of Fig. 2(e) without an appreciable topological change in the disclination lines. Therefore the two states are reversibly switchable to each other, though the one shown in Fig. 2(i) is metastable as shown below.

In Figs. 3(g) to 3(n), we show how the relaxation process depends on when the field is switched off in the case of $E = 20$ V/μm. When the field is switched off at $t/\tau_\chi = 5.80$

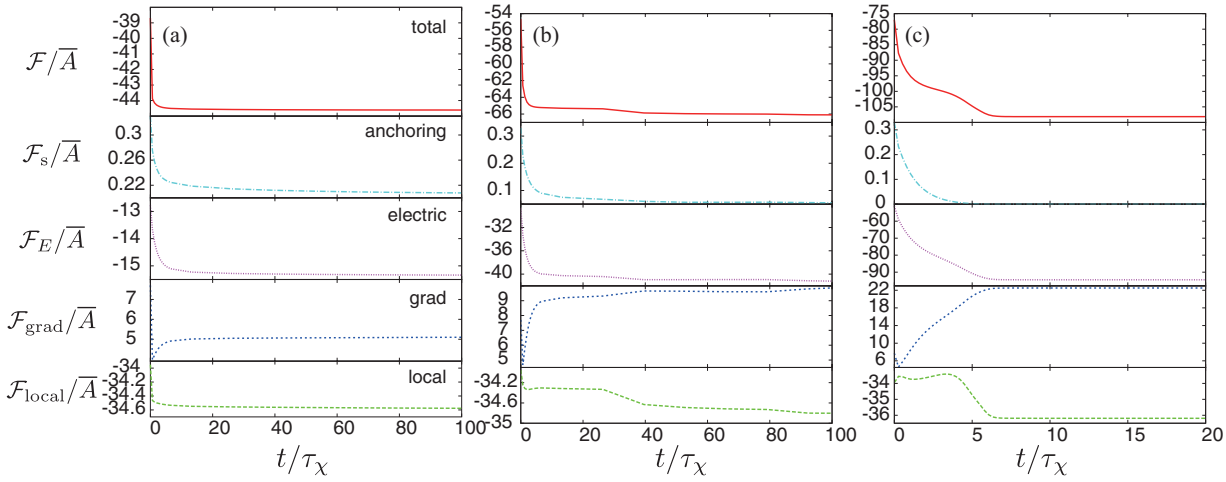

FIG. 5. (Color online) Time evolution of the total free energy per unit area $\mathcal{F}/\overline{A}$ (labeled by "total"), and each contribution from the local ($\mathcal{F}_{\rm local}/\overline{A}$, "local"), gradient ($\mathcal{F}_{\rm grad}/\overline{A}$, "grad"), electrostatic ($\mathcal{F}_E/\overline{A}$, "electric"), and anchoring ($\mathcal{F}_s/\overline{A}$, "anchoring") energies for $E =$ (a) 10, (b) 15, and (c) 20 V/μm. Only the range of t/τ_χ where these energies show notable changes is shown.

before the liquid crystal attains a uniform profile [see Fig. 3(d)], the disclination lines of square appearance emerge just after the cessation of the field [Fig. 3(g)], and then we see undulating disclination lines near the cell surfaces and those of a winding form around the midplane [Fig. 3(h)]. The winding disclination lines widen, become helical, and eventually merge [Fig. 3(i)] and form a highly entangled disclination network [Fig. 3(j)]. We also note that the shape of the surface defects is different from that of the initial profile before the application of an electric field. If the field is switched off at $t/\tau_\chi = 13.2$ when the orientational order of the liquid crystal is almost uniform [see Fig. 3(e)], the relaxation process is quite different: loop disclinations suddenly appear after some incubation time [Fig. 3(k)], and then they expand and form helical order locally as the time elapses [Fig. 3(l)]. The disclinations are nucleated from small fluctuations that exist in the initial conditions and remain even after their suppression by the strong field. The creation of loop disclinations reminds us of the formation of ring-like disclinations in a thin cell of a chiral liquid crystal where frustrations are introduced by confining surfaces imposing strong planar anchoring [24]. These helical defects merge, and again eventually form highly entangled disclinations [Figs. 3(m) and 3(n)]. In contract to the previous case, the disclination lines reach the cell surfaces, which is allowed in our case of finite surface anchoring. In our calculation, the system does not recover the BP-I-like regular network of disclination line that would require much longer time. In numerical calculations based on the discretization of continuum equations, it is quite difficult to achieve a periodic structure with no irregularity without preparing an appropriate initial condition. Adding a thermal fluctuation term in the dynamical equation does not facilitate the formation of perfectly regular structures, as demonstrated in Ref. [31] where the dynamics of microphase separation in block copolymers was discussed.

In Fig. 6, we show the time evolution of $\overline{\chi}_{zz}$ after the field is switched off. In the cases of $E = 10$ and 15 V/μm, $\overline{\chi}_{zz}$ exhibits a sharp but continuous drop followed by a gradual decrease towards an equilibrium value. The smooth variation of $\overline{\chi}_{zz}$ without kinks reflects the absence of topological change in the disclination network. In the former case, the equilibrium value of $\overline{\chi}_{zz}$ is exactly the same as the initial value 0.082, consistent with the fact that the disclination network recovers its original profile sufficiently after the field is switched off.

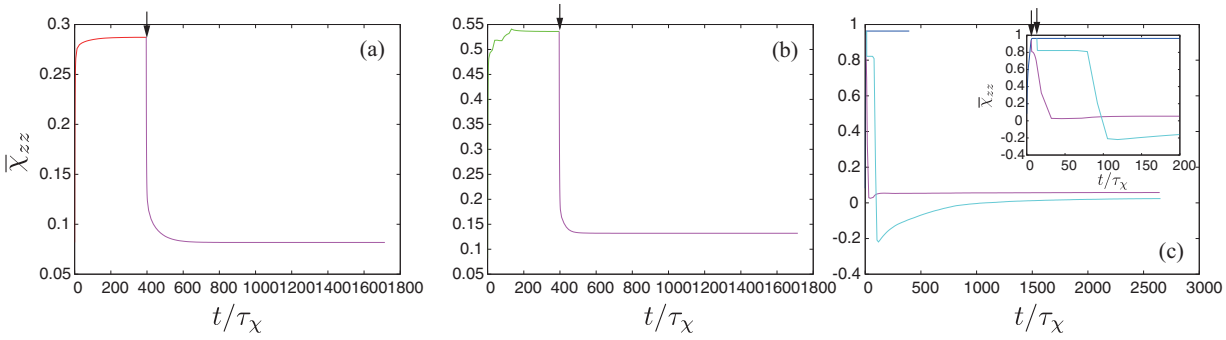

FIG. 6. (Color online) Time evolution of $\overline{\chi}_{zz}$ for $E =$ (a) 10, (b) 15, and (c) 20 V/μm before and after the field is switched off. The time when the field is switched off is indicated by an arrow. Two curves in (c) correspond to the time evolutions presented in Figs. 3(g) to 3(j) and Figs. 3(k) to 3(n). Inset in (c) shows the initial stage from $t/\tau_\chi = 0$ to 200.

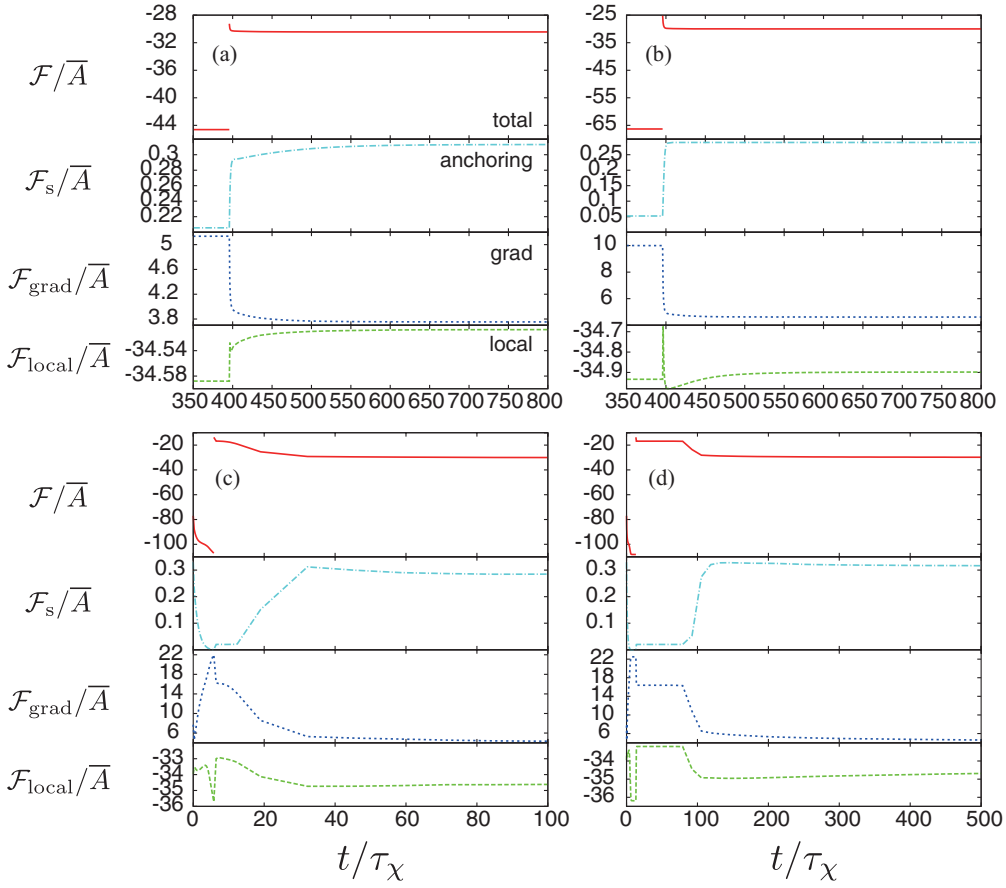

FIG. 7. (Color online) Time evolution of the total free energy per unit area $\mathcal{F}/\overline{A}$ (labeled by "total"), and each contribution from the local ($\mathcal{F}_{local}/\overline{A}$, "local"), gradient ($\mathcal{F}_{grad}/\overline{A}$, "grad"), and anchoring ($\mathcal{F}_s/\overline{A}$, "anchoring") energies for the field $E =$ (a) 10, (b) 15, and (c,d) 20 V/μm before and after the field is switched off. The discontinuity of $\mathcal{F}/\overline{A}$ marks the time when the field is switched off [$t/\tau_\chi = 396$ for (a,b), 5.80 for (c), and 13.2 for (d)]. Only the range of t/τ_χ where these energies show notable changes is shown.

In the latter case, a small change in the topology of the disclination network in Fig. 2 manifests itself in a relatively rapid approach of $\overline{\chi}_{zz}$ to the equilibrium value compared to the case of $E = 10$ V/μm. Time evolution of $\overline{\chi}_{zz}$ is more complex in the cases of $E = 20$ V/μm. Again kinks in the time evolution of $\overline{\chi}_{zz}$ [Fig. 6(c)] for the case of earlier cessation of the field [the time evolution of the disclination profile given in Figs. 3(g) to 3(j)] reflect the change in the topology of the disclination networks. In the case of later cessation [corresponding to Figs. 3(k) to 3(n)], one can clearly see a metastable state with large $\overline{\chi}_{zz}$, followed by a sudden decrease initiated by the nucleation of defects [Fig. 3(k)]. It is interesting that $\overline{\chi}_{zz}$ becomes negative after the sudden decrease. The profile in Fig. 3(l) contains an irregular array of disclinations of helical form. In a preliminary calculation for negative ϵ_a now shown here, we find that a regular array of helical disclination with negative $\overline{\chi}_{zz}$. Therefore, a negative $\overline{\chi}_{zz}$ in the case of Fig. 6(c) could be attributed to the formation of helical disclinations.

In Fig. 7, we show the time evolution of $\mathcal{F}/\overline{A}$, $\mathcal{F}_{local}/\overline{A}$, $\mathcal{F}_{grad}/\overline{A}$, and $\mathcal{F}_s/\overline{A}$ before and after the field is switched off ($\mathcal{F}_E/\overline{A}$ is not shown because $\mathcal{F}_E/\overline{A} = 0$ after the field

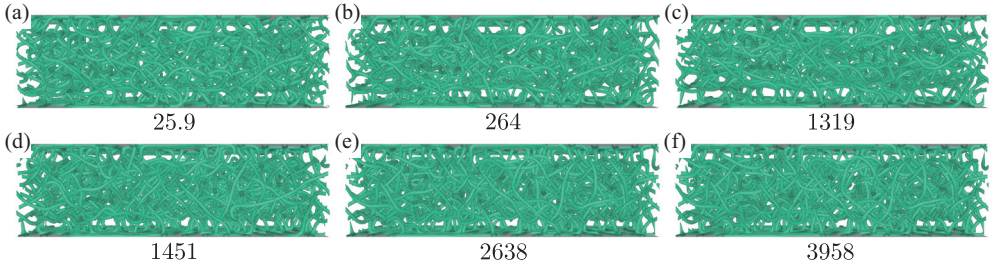

FIG. 8. (Color online) (a–c) Time evolution of disclination lines when the field $E = 10$ V/μm is applied to the profile of Fig. 3(n) at $t/\tau_\chi = 0$. (d–f) Time evolution of disclination lines after the field is switched off at $t/\tau_\chi = 1319$. Here and in Figs. 9 and 10 the numbers indicate t/τ_χ after the field is switched on.

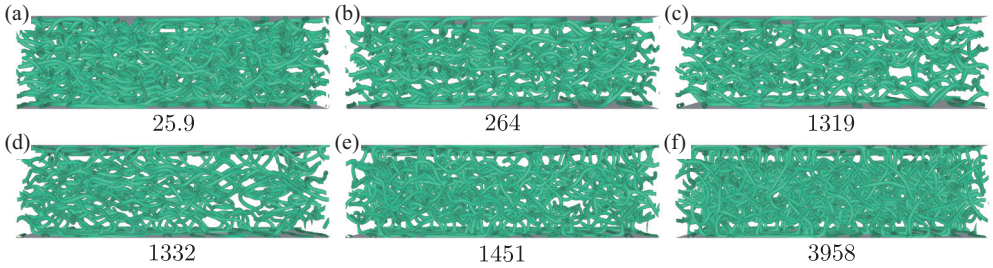

FIG. 9. (Color online) (a–c) Time evolution of disclination lines when the field $E = 15$ V/μm is applied to the profile of Fig. 3(n) at $t/\tau_\chi = 0$. (d–f) Time evolution of disclination lines after the field is switched off at $t/\tau_\chi = 1319$.

is switched off). As in the previous case under an applied field (Fig. 5), the variation of the elastic energy $\mathcal{F}_{\rm grad}$ dominates that of the total energy (again note the scale of the vertical axes). Moreover the variation of $\mathcal{F}$'s synchronizes that of $\overline{\chi}_{zz}$ shown in Fig. 4 [the synchronization is more clearly visible in $\mathcal{F}_{\rm grad}$, and in the cases of $E = 20$ V/μm in Figs. 7(c) and 7(d)]. The abrupt but continuous increase of $\mathcal{F}_s$ just after the field is switched off for $E = 10$ and 15 V/μm [Figs. 7(a) and 7(b)] arises from the widening of surface disclinations (see Figs. 1 and 2). In the cases of $E = 20$ V/μm in Figs. 7(c) and 7(d), one can notice, by comparing Figs. 3, 7(c), and 7(d) that $\mathcal{F}_s$ starts to increase when the disclinations reach the confining surfaces. Although the time evolution of $\mathcal{F}_{\rm local}$ is not easy to understand intuitively, the cessation of the electric field brings about the overshoot of $\mathcal{F}_{\rm local}$. In the case of $E = 10$ V/μm [Fig. 7(a)], the expansion of the disclination line network causes an increase of $\mathcal{F}_{\rm local}$. For $E = 20$ V/μm [Figs. 7(c) and 7(d)], the overshot $\mathcal{F}_{\rm local}$ seems to be relaxed by the emergence and evolution of disclination lines.

The total free energy of the system per unit area $\mathcal{F}/\overline{A}$ sufficiently after the field is switched off is, in the rescaled units presented in Sec. II, -30.44, -29.99 for the cases of $E = 10$ and 15 V/μm, respectively. For the cases of $E = 20$ V/μm, $\mathcal{F} = -30.23$ and -30.12 when the field is switched off at $t/\tau_\chi = 5.80$ and 13.2, respectively. The value $\mathcal{F}/\overline{A} = -30.44$ is exactly the same as that of the initial condition before the introduction of randomness. The free energy difference $\Delta\mathcal{F}/\overline{A} = 1$ corresponds to $\Delta\mathcal{F}/\overline{A} \simeq 1.5 \times 10^{-4}$ Jm^{-2} $\simeq 3.6 \times 10^{16} k_B T$m^{-2} in dimensional units [26], where k_B is the Boltzmann constant and $T \simeq 300$ K is the absolute temperature. The dimension of the repeating unit of the disclination network is roughly equal to $p = 161$ nm. Therefore, when $\Delta\mathcal{F}/\overline{A} = 1$, the free energy difference per area of the repeating unit is $(\Delta\mathcal{F}/\overline{A})p^2 \simeq 0.94 \times 10^3 k_B T$. We thus conclude that the free energy of the structures equilibrated after the field of strength 15 or 20 V/μm is switched off is sufficiently larger than that of the initial profile (or, equivalently, that equilibrated after the field of 10 V/μm is switched off); the difference is about $200 k_B T$ or even more per area of the repeating unit. We note that in numerical calculations based on continuum descriptions, the estimation of the energy barrier between two (meta)stable states is highly complex and demanding because of the large number of degrees of freedom, and therefore is beyond the scope of the present work.

C. Response of the entangled disclination network

One might wonder how the entangled disclination network after the cessation of a strong electric field (shown in Fig. 3) behaves when the electric field is switched on again. We carry out simulations to figure out the response of the profile of Fig. 3(n) to the application and cessation of the field. These simulations correspond to cycling the field more than once. In this section, the time t is measured so that the field is applied to the entangled disclination network at $t = 0$.

In Fig. 8, we show the time evolution of the disclination profile when an electric field $E = 10$ V/μm is applied, and later switched off. Under an electric field, the disclination network shrinks towards the midplane of the cell [note the presence of more vacancies of disclination lines in Fig. 8(c)], though the disclination lines reach the cell surfaces and the entangled nature of the disclination network remains unchanged; as in the case of Fig. 1, the field is not strong enough to reorganize the disclinations drastically. After the field is switched off, the disclination network expands towards the cell surfaces. The behavior of the disclination lines is almost the same when the field strength is $E = 15$ V/μm

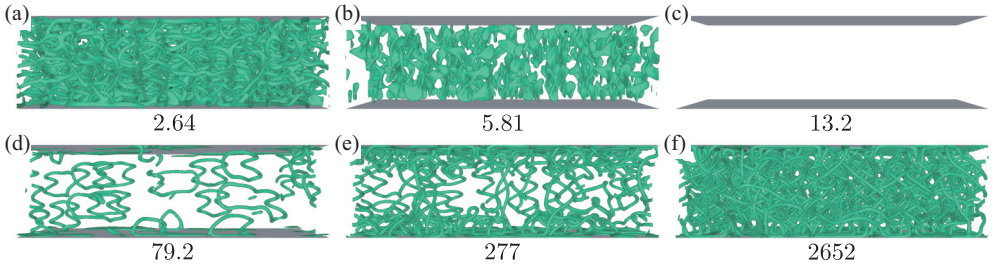

FIG. 10. (Color online) (a–c) Time evolution of disclination lines when the field $E = 20$ V/μm is applied to the profile of Fig. 3(n) at $t/\tau_\chi = 0$. (d–f) Time evolution of disclination lines after the field is switched off at $t/\tau_\chi = 13.2$.

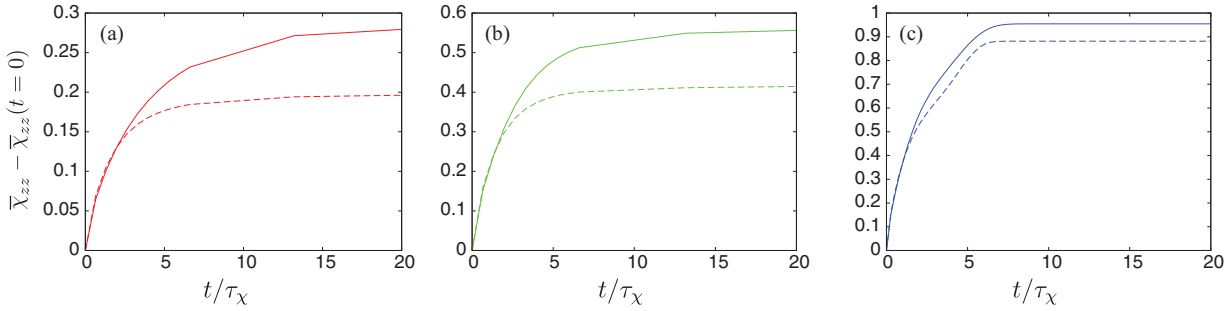

FIG. 11. (Color online) Time evolution of $\overline{\chi}_{zz}$ for $E =$ (a) 10, (b) 15, and (c) 20 V/μm. Solid lines are the results when the field is applied to the entangled disclinations [Fig. 3(n)], and dashed lines are those given in Fig. 4 (electric field is applied to the BP-I-like regular disclinations). Here $\overline{\chi}_{zz}$ is subtracted by $\overline{\chi}_{zz}(t=0)$, which is 0.0088 for the former case (solid lines), or 0.082 for the latter case (dashed lines).

(Fig. 9), though the density of the disclination lines becomes smaller when the field is applied.

As in the case of Fig. 3, a stronger field of $E = 20$ V/μm can align the liquid crystal along the field to eliminate disclination lines. We show the dynamics of the disappearance of the disclination lines in Fig. 10. Again when the field is switched off, disclination rings first appear after some incubation time, and then they evolve to form an entangled disclination network, as in the dynamics shown in Fig. 3.

In Fig. 11, we show the time evolution of $\overline{\chi}_{zz}$ from the entangled disclinations just after the field is applied to compare it to the time evolution shown in Fig. 4, that is, the response of a BP-I-like network of disclinations. For all cases with different E's, the initial evolution of $\overline{\chi}_{zz}$ looks almost the same irrespective of the initial condition. However, the evolution of $\overline{\chi}_{zz}$ is saturated later for the case of initial entangled disclinations, which results in larger final values of $\overline{\chi}_{zz}$; for $E = 10$ V/μm, $\overline{\chi}_{zz} = 0.307$ and 0.287 for entangled and regular initial conditions, respectively, and for $E = 15$ V/μm, $\overline{\chi}_{zz} = 0.632$ and 0.536. On the other hand, when $E = 20$ V/μm, $\overline{\chi}_{zz} = 0.963$ irrespective of the initial condition because in both cases the liquid crystal is uniformly aligned in the final state. The reason for larger $\overline{\chi}_{zz}$ might be that entangled disclinations respond more easily to an applied field than BP-I-like regular disclinations because of their metastability with regions with larger local free energies.

Figure 12 presents the time evolution of $\overline{\chi}_{zz}$ after the electric field is switched off, together with, for reference, the time evolution shown in Fig. 6 where the initial electric field was applied to BP-I-like regular disclinations. In the cases of $E =$ 10 and 15 V/μm, the time evolution of $\overline{\chi}_{zz}$ is slower than that given in Fig. 6, although the difference is small. This is because entangled disclinations relax inhomogeneously owing to their nonuniform structures, while the liquid crystal profiles in the previous cases (Figs. 1, 2, and 6), retains regularity, or spatial periodicity, and the relaxation of the system can be almost homogeneous and fast. Figure 12(c) demonstrates the time evolution of $\overline{\chi}_{zz}$ quite similar to that in Fig. 6(d) when the field $E = 20$ V/μm is switched off. This is natural because in both cases the profile of the liquid crystal just before the cessation of the field is uniform.

The time evolution of free energy contributions after the field is applied is given in Fig. 13. In the case of $E = 10$ V/μm, the comparison between Figs. 13(a) and 5(a) reveals that the relaxation of the free energy is considerably slower for entangled disclinations, which was not clearly visible in the time evolution of $\overline{\chi}_{zz}$ [Fig. 11(a)]. As in the previous case shown in Fig. 5, the relaxation of the total energy is dominated by those of $\mathcal{F}_E$ and $\mathcal{F}_{\rm grad}$, and the slower relaxation is clearly visible in these two contributions as well as in $\mathcal{F}_{\rm local}$. The results in Figs. 11(a) and 13(a) indicate that the entangled disclination lines allow larger variation of $\overline{\chi}_{zz}$ and hence larger birefringence, although the dynamics under the field is slow

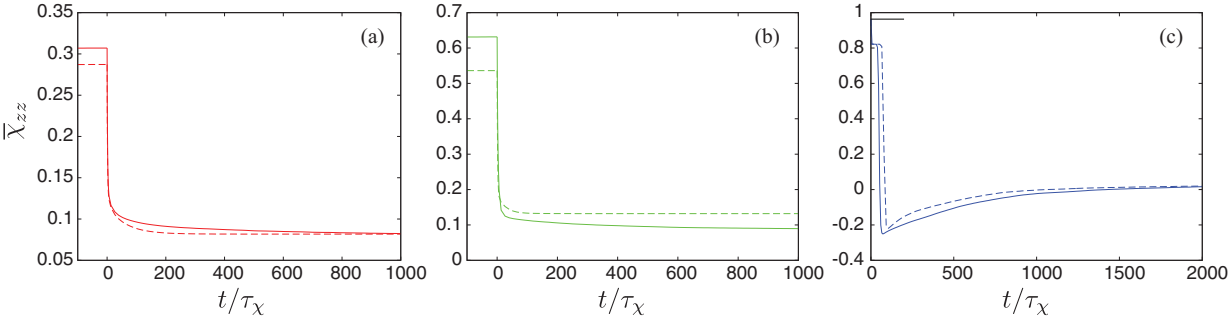

FIG. 12. (Color online) Time evolution of $\overline{\chi}_{zz}$ when the field $E =$ (a) 10, (b) 15, and (c) 20 V/μm is switched off at $t/\tau_\chi = 0$. Solid lines are the results when the field is first applied to the entangled disclinations [Fig. 3(n)], and dashed lines are those given in Fig. 6 (electric field is first applied to the BP-I-like regular disclinations and switched off). In (c), the value of $\overline{\chi}_{zz}$ just before the cessation of the field (0.963 in both cases) is highlighted by a short horizontal line.

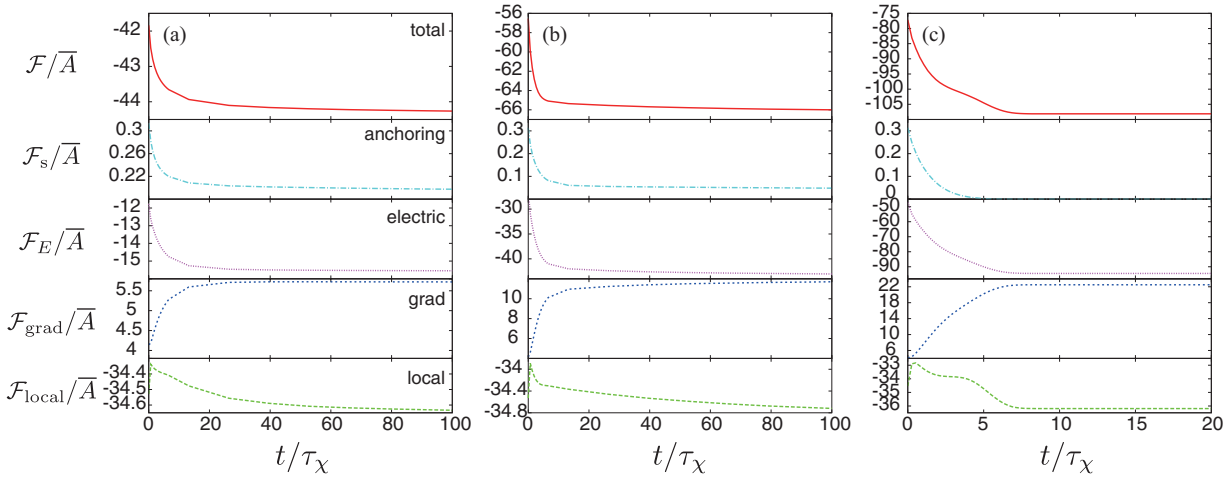

FIG. 13. (Color online) Time evolution of the total free energy per unit area $\mathcal{F}/\overline{A}$ (labeled by "total"), and each contribution from the local ($\mathcal{F}_{\rm local}/\overline{A}$, "local"), gradient ($\mathcal{F}_{\rm grad}/\overline{A}$, "grad"), electrostatic ($\mathcal{F}_E/\overline{A}$, "electric"), and anchoring ($\mathcal{F}_s/\overline{A}$, "anchoring") energies for $E =$ (a) 10, (b) 15, and (c) 20 V/μm when the field is applied to the profile given in Fig. 3(n). Only the range of t/τ_χ where these energies show notable changes is shown.

because the field has to act on irregular disclination lines. On the other hand, in the case of $E = 15$ V/μm, $\mathcal{F}$'s in Fig. 13(b) do not exhibit considerable slow relaxation compared with that of Fig. 5(b). However, the kinks in Fig. 5(b) characterizing the rearrangement of disclination lines cannot be seen in Fig. 13(b) because the reorganization of entangled disclination lines occurs continually everywhere in the system, which smears out the kinks in the time evolution of $\mathcal{F}$'s. It is interesting to find that the result given in Fig. 13(c) for $E = 20$ V/μm is almost indistinguishable from that in Fig. 5(c) for a BP-I-like initial profile, except for the time evolution of $\mathcal{F}_{\rm local}$ in the very initial stage. Under this strong field, the liquid crystal is eventually oriented along the field direction leading to the disappearance of disclination lines, and the process of this strong alignment is insensitive to initial conditions.

In Fig. 14, we show how $\mathcal{F}$'s evolve after the electric field is switched off. As in the previous case shown in Fig. 7, the temporal variation of $\mathcal{F}_{\rm grad}$ dominates that of the total free energy for all E's. For $E = 10$ V/μm, a comparison between Figs. 14(a) and 7(a) does not reveal a significant difference, although after the relaxation $\mathcal{F}_{\rm grad}$ is smaller for the latter case, which is attributable to entangled disclinations in the former case. For the case of $E = 15$ V/μm as well, the slower relaxation of $\mathcal{F}_{\rm grad}$ and $\mathcal{F}_s$ for entangled disclinations is visible from the comparison between Figs. 14(b) and 7(b). As in the time evolution of $\overline{\chi}_{zz}$ shown in Fig. 12(c), the time evolution of $\mathcal{F}$'s after the field $E = 20$ V/μm is switched off in Fig. 14(c) is quite similar to that given in Fig. 7(d).

The total free energy per unit area $\mathcal{F}/\overline{A}$ sufficiently after the field is switched off is -30.20, -30.17, and -30.12 for $E = 10$, 15, and 20 V/μm, respectively, while that of the initial state with entangled disclination is -30.12 (see Sec. III B). According to the discussion in Sec. III B, the free energy difference between the initial state ($\mathcal{F}/\overline{A} = -30.12$)

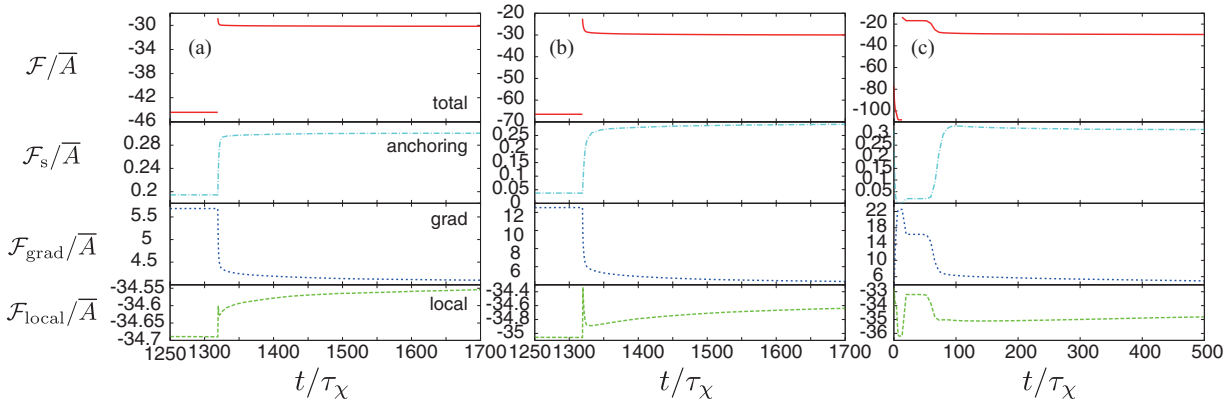

FIG. 14. (Color online) Time evolution of the total free energy per unit area $\mathcal{F}/\overline{A}$ (labeled by "total"), and each contribution from the local ($\mathcal{F}_{\rm local}/\overline{A}$, "local"), gradient ($\mathcal{F}_{\rm grad}/\overline{A}$, "grad"), and anchoring ($\mathcal{F}_s/\overline{A}$, "anchoring") energies for the field $E =$ (a) 10, (b) 15, and (c) 20 V/μm before and after the field is switched off, when the field is initially applied to the profile given in Fig. 3(n). The discontinuity of $\mathcal{F}/\overline{A}$ marks the time when the field is switched off [$t/\tau_\chi = 1319$ for (a,b) and 13.2 for (d)]. Only the range of t/τ_χ where these energies show notable changes is shown.

and the final state per unit area of a repeating regular disclination network ($\sim p^2$) is a few tens of k_BT for $E = 10$ and 15 V/μm. Although this difference is smaller than that between a regular disclination network and an entangled one, this result indicates that apparently indistinguishable entangled disclination networks can have sufficiently different free energies. In the case of $E = 20$ V/μm, the free energy after the relaxation is almost identical for the two simulations, which is reasonable because in both simulations the liquid crystal is uniformly aligned when the field is switched off.

IV. CONCLUSION

We investigated the dynamics of a cholesteric blue phase cell made up of a chiral liquid crystal confined by parallel surfaces, by numerical calculations based on a Landau–de Gennes theory describing the orientational order by a second-rank tensor order parameter. We focused on its response to an electric field applied between the confining cell surfaces. We demonstrated that the dynamics of the disclination lines in the liquid crystal depends sensitively on the field strength and the history of the application of the electric field. When the field is not strong, the disclination network inherent in a cholesteric blue phase just shrinks along the field direction without its topology being changed. However, stronger field brings about complex reorganization processes of disclination lines, and the final profile can be disclination lines of different shape localized around the midplane of the cell, or a uniform alignment along the field direction with no disclination lines.

We also studied the relaxation dynamics of the cell when the field is switched off. Again the relaxation process and the resulting profile strongly depend on the initial profile of the cell just before the cessation of the field. A compressed disclination network of BP I in the case of weak field ($E = 10$ V/μm) simply recovers the original profile, exhibiting reversible switching between two states. Also a switching between metastable states was found in the case of $E = 15$ V/μm. However, the orientation profiles strongly influenced by a stronger field ($E = 20$ V/μm) exhibit nontrivial and complex reorganization processes, depending sensitively on the initial profile of the relaxation. In particular, we found the spontaneous formation of an entangled disclination network when the field is switched off from a liquid crystal uniformly aligned by a strong field. The complexity of the relaxation processes manifested itself also when the entangled disclination lines mentioned above are used as an initial condition. We found the relaxation of entangled disclinations slower than that of regular BP-I-like ones, which is natural considering the irregular profile of entangled disclinations.

We believe that we have succeeded in demonstrating rich behaviors of a cholesteric blue phase cell in response to an applied electric field. Some of them, including the compression of the disclination network due to the enhanced normal alignment of the liquid crystal near the confining surfaces, and the nucleation of disclinations near the surface when the field is switched off, are specific to a cell and not observed in the bulk. Although direct experimental observation of the real-space orientation profile of blue phase materials still remains a challenge, a successful observation of the lattice structures of BP I using confocal microscopy was recently reported [32]. Therefore we hope that the present study will stimulate further experimental study aiming at direct observation of the dynamics of cholesteric blue phases in a planar cell. The great advantage of our numerical scheme is that the electric field is calculated by the Poisson equation with the spatial distribution of the dielectric tensor taken into account explicitly, instead of an assumption of a uniform field in previous studies on the same subject. Though in the present study the profile of the electric field is almost uniform and thus this advantage is of minor importance, our scheme will be quite powerful when the electric field is far from uniform because of the design of electrodes. Considering the recent growing interest in the application of a cholesteric blue phase to fast-switching displays, we believe that our scheme will help investigate the dynamics of a cholesteric blue phase cell and propose designs of a cell for a more efficient use of the properties of cholesteric blue phases.

ACKNOWLEDGMENTS

J.F. thanks Professor Hirotsugu Kikuchi for valuable discussions and encouragement. We appreciate the support of the Slovenian Research Agency (ARRS research program P1-0099 and project J1-2335), and the Center of Excellence NAMASTE, which enabled J.F. to stay at the University of Ljubljana and carry out part of this work there. J.F. is also supported by KAKENHI for Young Scientists (23740324) from Japan Society for the Promotion of Science, and the Cooperative Research Program of "Network Joint Research Center for Materials and Devices."

APPENDIX: RESCALING OF THE VARIABLES

Here we present how relevant parameters are rescaled. The rescaling of $f_{\rm local}$ and $f_{\rm grad}$ is exactly the same as that presented in Ref. [1]. The rescaled free energy densities and order parameter read $\varphi_{\rm local,grad} \equiv (a^3/b^4) f_{\rm local,grad}$, and $\chi_{\alpha\beta} \equiv (a/b) Q_{\alpha\beta}$. The lengths are measured in units of $(2q_0)^{-1}$ and the rescaled spatial derivative reads $\overline{\nabla} = (2q_0)^{-1}\nabla$. We also have the relations $\tau \equiv (a/b^2)c$, $\kappa \equiv \sqrt{aK_1q_0^2/b^2}$ and $\eta \equiv K_0/K_1$. τ is now assumed to depend linearly on temperature, and thus safely called the rescaled temperature. Though κ is closely related to the elastic constant, it is proportional to q_0 and thus measures the strength of chirality. For the rescaling of φ_s to be consistent, the rescaled anchoring strength should be $w \equiv 2q_0(a/b^2)W$. We employ the following typical values for the material parameters [23]; $a \simeq 8 \times 10^4$ Jm^{-3}, $b \simeq 5 \times 10^4$ Jm^{-3}, $K_1 \simeq 10$ pN, and $c = \tilde{c}(T - T^*)$ with $\tilde{c} = 3 \times 10^4$ Jm^{-3} K^{-1}, T being the temperature of the liquid crystal in Kelvin and T^* being the temperature below which an isotropic state becomes unstable with respect to small perturbations. Then the rescaled temperature becomes $\tau \simeq 1 \times (T - T^*)$, and the cholesteric pitch becomes $2\pi/q_0 \simeq 113/\kappa$ nm. The anchoring strength is $W \simeq w \times 4 \times 10^{-4}$ Jm^{-3}. We note that other choices of a, b, $\tilde{c}$, K_1 yield different relations between q_0 and κ, between T and τ, and between W and w.

We employ the same rescaling for the electrostatic energy density so that $\varphi_E \equiv (a^3/b^4) f_E$. When we consider a uniaxial nematic with the director $\boldsymbol{n}$ so that $\epsilon_{\alpha\beta}$ is also uniaxial with its symmetry axis being $\boldsymbol{n}$, $\epsilon_{\alpha\beta}$ is written as $\epsilon_{\alpha\beta}/\epsilon_0 = (\epsilon_{||} - \epsilon_\perp) n_\alpha n_\beta + \epsilon_\perp \delta_{\alpha\beta}$, with $\epsilon_{||}$ and $\epsilon_\perp$ being the component of $\epsilon_{\alpha\beta}$ along and perpendicular to $\boldsymbol{n}$, respectively. ϵ_0 is the vacuum permittivity. The part of the electrostatic free energy density dependent on $\boldsymbol{n}$ is now given by [27]

$$f_E = -\tfrac{1}{2}\epsilon_0 \epsilon_a (\boldsymbol{E}\cdot\boldsymbol{n})^2, \tag{A1}$$

where we have defined $\epsilon_a \equiv \epsilon_{||} - \epsilon_\perp$. When we adopt a uniaxial form of the order parameter, $\chi_{\alpha\beta} = \chi_0 (n_\alpha n_\beta - (1/3)\delta_{\alpha\beta})$, and compare Eqs. (A1) and (8), we have

$$\overline{E} = \sqrt{(a^3/\chi_0 b^4)\epsilon_0} E. \tag{A2}$$

When we assume $\chi_0 \simeq 1$ and measure E in units of V/μm, we arrive at Eq. (11). Note also that when $\chi_0 = 1$, $\epsilon_{\rm iso} = (\epsilon_{||} + 2\epsilon_\perp)/3$.

The values $\epsilon_{\rm iso}$ and ϵ_a strongly depend on materials, and in our calculation we set $\epsilon_{\rm iso} = 10$, and $\epsilon_a = 10$. Information on the values of $\epsilon_{||}$ and $\epsilon_\perp$ for blue phase materials was not available, and therefore we employed $\epsilon_{||} \simeq 17$ and $\epsilon_\perp \simeq 7$ for a typical nematic liquid crystal 5CB [33,34]. A typical value of ϵ_a for blue phase materials is $\epsilon_a \simeq 7$ [35], and therefore the above choice of $\epsilon_{\rm iso}$ and ϵ_a is reasonable. We also note that as long as $\epsilon_{\rm iso} E^2$ and $\epsilon_a E^2$ remain the same, the dynamics presented in the main text remains unaltered irrespective of the choice of $\epsilon_{\rm iso}$ and ϵ_a.

When the absolute value of the negative eigenvalue of $\chi_{\alpha\beta}$ is extremely large, the electrostatic energy φ_E is not positive definite. In our calculations we do not encounter such situations.

[1] D. C. Wright and N. D. Mermin, Rev. Mod. Phys. **61**, 385 (1989).
[2] P. P. Crooker, in *Chirality in Liquid Crystals*, edited by H.-S. Kitzerow and C. Bahr, Chap. 7 (Springer, Berlin, 2001).
[3] O. Henrich, K. Stratford, M. E. Cates, and D. Marenduzzo, Phys. Rev. Lett. **106**, 107801 (2011).
[4] H. Kikuchi, M. Yokota, Y. Hisakado, H. Yang, and T. Kajiyama, Nat. Mater. **1**, 64 (2002).
[5] H. J. Coles and M. N. Pivnenko, Nature (London) **436**, 997 (2005).
[6] A. Yoshizawa, M. Sato, and J. Rokunohe, J. Mater. Chem. **15**, 3285 (2005).
[7] W. Cao, A. Muñoz, P. Palffy-Muhoray, and B. Taheri, Nat. Mater. **1**, 111 (2002).
[8] S. Yokoyama, S. Mashiko, H. Kikuchi, K. Uchida, and T. Nagamura, Adv. Mater. **18**, 48 (2006).
[9] Samsung Electronics Co., Ltd., "15inch Blue Phase Mode LC Display," presented at SID2008, Los Angeles (2008).
[10] Z. Ge, S. Gauza, M. Jiao, H. Xianyu, and S.-T. Wu, Appl. Phys. Lett. **94**, 101104 (2009).
[11] H. Choi, H. Higuchi, and H. Kikuchi, Appl. Phys. Lett. **98**, 131905 (2011).
[12] Y. Hisakado, H. Kikuchi, T. Nagamura, and T. Kajiyama, Adv. Mater. **17**, 96 (2005).
[13] D. K. Yang, J. W. Doane, Z. Yaniv, and J. Glasser, Appl. Phys. Lett. **64**, 1905 (1994).
[14] H.-S. Kitzerow, Mol. Cryst. Liq. Cryst. **202**, 51 (1991).
[15] A. Dupuis, D. Marenduzzo, and J. M. Yeomans, Phys. Rev. E **71**, 011703 (2005).
[16] G. P. Alexander and J. M. Yeomans, Phys. Rev. E **74**, 061706 (2006).
[17] G. P. Alexander and D. Marenduzzo, EPL **81**, 66004 (2008).
[18] J. Fukuda, M. Yoneya, and H. Yokoyama, Phys. Rev. E **80**, 031706 (2009).
[19] O. Henrich, D. Marenduzzo, K. Stratford, and M. E. Cates, Phys. Rev. E **81**, 031706 (2010).
[20] A. Tiribocchi, G. Gonnella, D. Marenduzzo, and E. Orlandini, Soft Matter **7**, 3295 (2011); A. Tiribocchi, G. Gonnella, D. Marenduzzo, E. Orlandini, and F. Salvadore, Phys. Rev. Lett. **107**, 237803 (2011).
[21] J. Fukuda and S. Žumer, Proc. SPIE **8279**, 82790V (2012).
[22] J. Fukuda and S. Žumer, Phys. Rev. Lett. **104**, 017801 (2010).
[23] J. Fukuda and S. Žumer, Liq. Cryst. **37**, 875 (2010).
[24] J. Fukuda and S. Žumer, Phys. Rev. Lett. **106**, 097801 (2011).
[25] J. Fukuda and S. Žumer, Nat. Commun. **2**, 246 (2011).
[26] J. Fukuda and S. Žumer, Phys. Rev. E **84**, 040701(R) (2011).
[27] P. G. de Gennes and J. Prost, *The Physics of Liquid Crystals*, 2nd ed. (Oxford University Press, Oxford, 1993).
[28] W. H. Press, S. A. Teukolsky, W. T. Vetterling, and B. P. Flannery, *Numerical Recipes*, 3rd ed. (Cambridge University Press, Cambridge, England, 2007).
[29] S. R. Fulton, P. E. Ciesielski, and W. H. Schubert, Mon. Wea. Rev. **114**, 943 (1986).
[30] We tried to quantify the compression of the disclination network by calculating $\mathrm{Tr}\mathbf{Q}^2_{\rm min}(z)$, the minimum value of $\mathrm{Tr}\mathbf{Q}^2$ for fixed z. When we define the disclination network by the region with $\mathrm{Tr}\mathbf{Q}^2_{\rm min}(z) < 0.6$, the compression along the z direction by the field $E = 10$ V/μm is approximately 19%. However, this quantity characterizing the compression could sensitively depend on the definition of the disclination network.
[31] S. R. Ren and I. W. Hamley, Macromolecules **34**, 116 (2001).
[32] K. Higashiguchi, K. Yasui, and H. Kikuchi, J. Am. Chem. Soc. **130**, 6326 (2008).
[33] P. G. Cummins, D. A. Dunmur, and D. A. Laidler, Mol. Cryst. Liq. Cryst. **30**, 109 (1975).
[34] B. R. Ratna and R. Shashidhar, Pramana **6**, 278 (1976).
[35] G. Heppke, B. Jerôme, H.-S. Kitzerow, and P. Pieranski, J. Phys. (France) **50**, 549 (1989).